

## A Staggered Grid Method for Solving Incompressible Flow on Unstructured Meshes

Huawen Shu, Minghai Xu, Xinyue Duan\*, Yongtong Li, Yu Sun, Ruitian Li and Peng Ding

College of New Energy, China University of Petroleum (East China), Qingdao, 266580, China

\*Corresponding Author: Xinyue Duan. Email: duanxy@upc.edu.cn

Received: 11 October 2019; Accepted: 03 January 2020

**Abstract:** A finite volume method based unstructured grid is presented to solve the two dimensional viscous and incompressible flow. The method is based on the pressure-correction concept and solved by using a semi-staggered grid technique. The computational procedure can handle cells of arbitrary shapes, although solutions presented in this paper were only involved with triangular and quadrilateral cells. The pressure or pressure-correction value was stored on the vertex of cells. The mass conservation equation was discretized on the dual cells surrounding the vertex of primary cells, while the velocity components and other scale variables were saved on the central of primary cells. Since the semi-staggered arrangement can't guarantee a strong coupling relationship between pressure and velocity, thus a weak coupling relationship leads to the oscillations for pressure and velocity. In order to eliminate such an oscillation, a special interpolation scheme was used to construct the pressure-correction equation. Computational results of several viscous flow problems show good agreement with the analytical or numerical results in previous literature. This semi-staggered grid method can be applied to arbitrary shape elements, while it has the most efficiency for triangular cells.

**Keywords:** Staggered grid; incompressible flow; pressure correction; finite volume method

### Nomenclature

$\overrightarrow{A_{cross}}$	cross diffusion coefficient
$\overrightarrow{A_f}, \overrightarrow{A_g}$	area vector
$a$	thermal diffusion coefficient
$a_i, a_j, b_i$	coefficients of discrete pressure-correction equation
$a_p, a_f, b$	coefficients of discrete convective diffusion equation
$c_p$	specific heat at constant pressure
$d_u, d_v$	pressure coefficient
$g$	gravitational acceleration
$H$	height of square cavity
$\vec{i}, \vec{j}$	unit vector



This work is licensed under a Creative Commons Attribution 4.0 International License, which permits unrestricted use, distribution, and reproduction in any medium, provided the original work is properly cited.

$m$	mass flux
$N$	the number of calculating cells
$NE$	the number of velocity cells
$N_f, N_g$	the number of interfaces
$NP$	the number of pressure cells
$Nu$	nusselt number
$p$	pressure
$Ra$	rayleigh number
$Re$	reynolds number;
$p$	pressure
$s$	source item
$T$	temperature
$u, v$	velocity component
$\vec{V}$	velocity vector
$x, y$	coordinate

### Greek symbols

$\alpha$	coefficient of thermal expansion
$\alpha_u, \alpha_v$	under-relaxation factor for velocity
$\alpha_p$	under-relaxation factor for pressure
$\Delta$	cell volume
$\Gamma$	diffusion coefficient
$\varphi$	general variable
$\rho$	density
$\theta$	angle
$\nu$	kinematic viscosity
$\lambda$	thermal conductivity

### Subscripts

$c$	low temperature
$f, g$	interface of control volume
$F, P$	velocity and other variables location
$i, j, k$	pressure location
$h$	high temperature
$V$	volume

### Superscripts

$c$	constant
$p$	slope
*	momentum equation solution

## 1 Introduction

Numerical simulations of fluid flow and heat transfer have been paid much attention, which is also becoming an essential tool for various industrial designs [1]. Unstructured triangular mesh is widely used in computational fluid dynamics and numerical heat transfer, because of its good adaptability to the complex boundaries and the convenience for automatic generation. Since the staggered strategy is much more complex on unstructured grids, the collocated grid is generally adopted for solving incompressible Navier-Stokes equations on unstructured grids, while the coupling relationship between pressure and

velocity is achieved through momentum interpolation method proposed by Rhie et al. [2]. There are many strategies that were proposed in the mid-1990s [3,4,5,6] and recent years [18,19,20]. Although the problem of pressure saw-tooth wave is eliminated in the early momentum interpolation techniques, the numerical results are dependent on the magnitude of the sub-relaxation factor or the time step of the velocity. In order to solve this problem, Yu et al. [7] proposed a modified momentum interpolation technique and the sub-relaxation factor or the time step independent numerical results were obtained. However, much more memory is needed in this technique to store the interface velocity information. Additionally, another problem of using the collocated grid method is that the velocity field served to satisfy the momentum equation is different from that satisfying the mass conservation equation, whether this inconsistency has an effect on the stability of the algorithm is unclear.

Aaron Katz et al. [8] examined the order of accuracy and error magnitude of the node-centered and cell-centered schemes on unstructured meshes and presented the flow field solutions for computational fluid dynamics. They found that the node-centered approaches produce less error than cell-centered approaches on isotropic grids. In contrast, for stretched meshes, cell-centered schemes are favored. Xue et al. [9] described a finite volume method for simulating transport processes governed by convection-diffusion type equations. The formulation is based on a cell-centered, unstructured grid. For the process of fluid flow modeling, a collocated arrangement of variables is employed to generate a single coefficient matrix that applies for each velocity component in the momentum equations.

Although the data structure of the unstructured staggered grid is relatively complex, this grid can naturally eliminate the decoupling phenomenon among velocity and pressure. Furthermore, the aforementioned discordant with two velocity fields does not exist in the staggered grid scheme. There have been some arrangements for variables in terms of the staggered grid in literature. Thomadakis et al. [10] proposed an arrangement with the velocity at the vertex of the cell and the pressure at the center of the cell. Compared with the traditional combination of velocity and pressure on a staggered grid, the coupling relationship between velocity and pressure is relatively feeble. Hwang et al. [11] presented a staggered grid method in which velocity is saved on the interface of cell, and pressure and other scalars are stored at the center of the cell. Peters et al. [12] also developed a special interpolation method to enhance the coupling between velocity and pressure based on the implement of velocity and pressure locations proposed in Hwang et al. [11]. The results match well with that of the original staggered grid. However, the expense of computation of this method is twice of the structured staggered grid. Since two velocity components are required to be solved at each interface, while there is only one velocity component in the structured grid system at one cell surface. If the original grid element is triangular, the number of sides is about 1.5 times the number of elements. Therefore, for the arrangement of velocity placed on the side of the cell, the computational cost for solving velocity is also about 1.5 times as that of the collocated grid arrangement.

In this paper, a semi-staggered grid with pressure at the vertex of cell and velocity and other scalars at the center of cell was developed. For the two-dimensional triangular mesh, the number of vertex is about half of the elements, thus the order of discrete pressure-correction equations can be reduced to half of the number of cells, which reduces the computation cost. Another advantage of this grid system is that the discretization of the mass conservation equation is automatically generated, without leading to a weak coupling relationship between velocity and pressure. The effectiveness of this method was verified by several numerical cases.

## 2 Governing Equations

The governing equations of steady-state incompressible Newton-fluid flow and heat transfer contain the conservation equations of mass, momentum and energy. The corresponding governing equations for the two-dimensional (2D) physical model can be written as follows:

$$\text{div}(\rho \vec{V}) = 0 \quad (1)$$

$$\text{div}(\rho \vec{V} u) = -\frac{\partial p}{\partial x} + \text{div}(\Gamma \text{grad} u) + s_u \quad (2a)$$

$$\text{div}(\rho \vec{V} v) = -\frac{\partial p}{\partial y} + \text{div}(\Gamma \text{grad} v) + s_v \quad (2b)$$

$$\text{div}(\rho \vec{V} \phi) = \text{div}(\Gamma \text{grad} \phi) + s_\phi \quad (3)$$

where the Eq. (3) is also known as the general convection-diffusion equation. It can express the governing equations of mass, momentum and other scalar quantities by giving the diffusion coefficient  $\Gamma$ , the source term  $s$ , and the general variable  $\Phi$  with specific physical meanings, respectively.  $\vec{V}$  and  $p$  stand for the velocity vector and pressure.  $\rho$  refers to the density of fluid. For example, Eq. (3) refers to the conservation equation of energy when  $\Phi = c_p T$  and  $\Gamma = \lambda$ .

### 3 Formulation of Discrete Equations

Fig. 1 shows the arrangement of the control volume for pressure and velocity, where the pressure is placed at the vertex of the cell, and the velocity and the other variables are arranged at the center of the cell. The area enclosed by the dotted line in Fig. 1 is the basic cell for the control volume of velocity and other scalars, where the solid points stand for positions of those variables. The polygon formed by solid lines is the control volume of pressure, where the hollow points locating at the vertex of the cell represent the position of pressure.

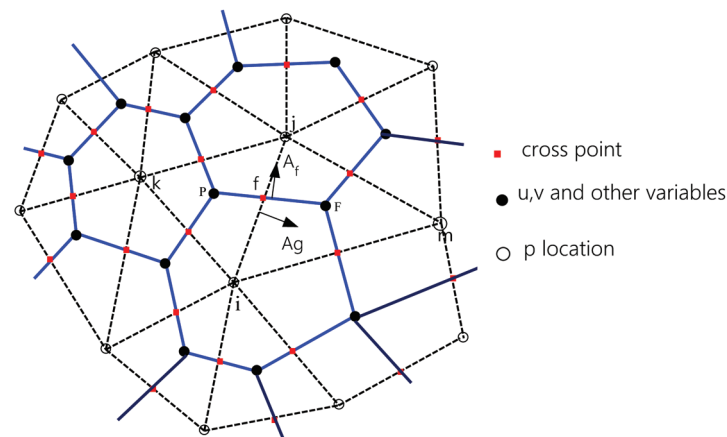


**Figure 1:** Control volumes for pressure and velocity components of  $u$  and  $v$

For this semi-staggered grid arrangement on triangular meshes, the ratio of the number of cell vertex, cells and cell boundaries is about 1:3:6, so the unknown number for pressure is about one-third of the collocated grid. But there are more unknowns in pressure (or pressure correction) equations and more multiplying operations for solving.

According to the Gauss-Green theorem and the assumption of the linear distribution of variables at the boundaries of control volume for the mass conservation equation, the integral of mass conservation equation can be written as:

$$\sum_f^{N_f} \left( (\rho \vec{V})_f \cdot \vec{A}_f \right) = \sum_f^{N_f} m_f = 0 \quad (4)$$

where  $\vec{A}_f$  represents the area vector of interface  $f$  of the control volume for pressure.  $N_f$  is the number of interface of the control volume for pressure. Eq. (4) shows that the discretization of the mass conservation equation depends on the calculation of mass flow  $m_f$  through the interface of the pressure control volume. Similarly, Gauss-Green theorem is adopted to discrete the general convection-diffusion equation to construct the discretized equation as shown in Eq. (5):

$$\sum_g^{N_g} \left( \rho \vec{V} \phi \right)_g \cdot \vec{A}_g = \sum_g^{N_g} (\Gamma \text{grad} \phi)_g \cdot \vec{A}_g + s_\phi \Delta_v \quad (5)$$

where  $\Delta_v$  is the volume of primary mesh (basic control volume).  $\vec{A}_g$  represents the area vector of interface  $g$  of the control volume.  $N_g$  is the number of control volume interfaces. The source item is linearized by  $s_\phi = s_\phi^c + s_\phi^p$ .

#### 4 Calculation of Convective Flux and Diffusion Flux

The convective flux in Eq. (5) is calculated by the second-order upwind scheme, while the over-relaxation technique presented by Jasak [11] is employed to calculate the diffusion flux in Eq. (5), as shown in Eqs. (6) and (7), respectively.

$$F_g^{conv} = (\rho \vec{v} \phi)_g \cdot \vec{A}_g = m_g \phi_g = m_g \left[ \phi_{up} + (\nabla \phi)_{up} \cdot \vec{r}_{upg} \right] \quad (6)$$

$$F_g^{diff} = (\Gamma \text{grad} \phi)_g \cdot \vec{A}_g = \Gamma_g D_F (\phi_F - \phi_P) + \Gamma_g \overline{\nabla \phi}_g \cdot \vec{A}_{cross} \quad (7)$$

where the subscript up represents the upstream cell, the subscript  $g$  stands for the midpoint boundary of the basic control volume,  $D_F = (\vec{A}_g \cdot \vec{A}_g) / (A_g / PF)$ ,  $\vec{PF} = (x_F - x_P, y_F - y_P)$ , the flux  $m_g$  flowing through the interface of control volume equals to  $(\rho \vec{v}) \cdot \vec{A}_g$ ,  $\vec{r}_{upg} = (x_g - x_{up}, y_g - y_{up})$ , the cross-diffusion coefficient resulted from the non-orthogonal of grid equals to  $\vec{A}_{cross} = (\vec{A}_g - D_F \vec{PF})$ , and  $\nabla \phi_g = \lambda (\nabla \phi)_P + (1 - \lambda) (\nabla \phi)_F$  is determined by using the least square method to calculate the gradient of cell. The discrete results of diffusion terms, convection terms and source terms are substituted into Eq. (5), the general discrete convective diffusion equation can be obtained as shown in Eqs. (8) and (9).

$$a_P \phi_P = \sum_F^{NF} a_F \phi_F + b \quad (8)$$

$$\begin{cases} a_F = \Gamma_g D_F + \max(0, -m_g) \\ a_P = \sum_F^{N_g} a_F - \Delta_v s_{\phi,P} \\ b = \sum_g^{N_g} \Gamma_g (\overline{\nabla \phi})_g \cdot \vec{A}_{cross} + \Delta_v s_\phi^c - \sum_g^{N_g} m_g \left[ (\nabla \phi)_{up} \cdot \vec{r}_{upg} \right]_g \end{cases} \quad (9)$$

Eq. (9) can be used to solve velocities, temperature and other scalar variables placed at the primary cell centers.

#### 5 Pressure-Correction Equation

Similar to Patankar's SIMPLE algorithm, that the velocity and pressure field satisfying the mass conservation equation also approximately matches the momentum conservation equation is assumed, while the corrective influence of velocity from adjacent cells is neglected. Based on the above

hypotheses, the relationship of the velocity satisfying the mass conservation equation and the pressure-corrections can be obtained:

$$\begin{cases} u_P = u_P^* - \frac{\Delta_v}{a_P} \left( \frac{\partial p'}{\partial x} \right)_P = u_P^* - d_u \left( \frac{\partial p'}{\partial x} \right)_P \\ v_P = v_P^* - \frac{\Delta_v}{a_P} \left( \frac{\partial p'}{\partial y} \right)_P = v_P^* - d_v \left( \frac{\partial p'}{\partial y} \right)_P \end{cases} \quad (10)$$

For the pressure control volume vertex  $i$  in Fig. 1, the mass flux flowing through  $PF$  can be divided into two parts, including the left flux flowing through  $Ff$  and the right flux flowing through  $fP$ . Since the defined position of velocity locates at point  $F$  and  $P$ , the values of velocity at those two points are used to calculate the flux through  $Ff$  and the flux through  $fP$ , respectively. Thus, the mass flux flowing through the interface  $f(PF)$  of pressure control volume in Eq. (4) can be written as:

$$m_f = \left( (\rho \vec{V})_f \cdot \vec{A}_f \right) = \left( (\rho \vec{V})_F \cdot \vec{A}_{f-Ff} \right) + \left( (\rho \vec{V})_P \cdot \vec{A}_{f-fP} \right) \quad (11a)$$

where Eq. (11a) shows that the mass flux calculation is almost the same as that of the original staggered grid, the difference is that the flux is computed from two velocities at the edge ends. In contrast, the mass flux is calculated from one velocity at the center of the edge for the original staggered grid method.

Then the velocity formula in Eq. (10) is substituted into Eq. (11a) to obtain the final formula of mass flow  $m_f$ :

$$\begin{aligned} m_f = m_{Ff} + m_{fP} = \rho_F \left[ \left( u_F^* - d_u \frac{\partial p'}{\partial x} \right)_F A_{f-Ff}^x + \left( v_F^* - d_u \frac{\partial p'}{\partial y} \right)_F A_{f-Ff}^y \right] \\ + \rho_P \left[ \left( u_P^* - d_u \frac{\partial p'}{\partial x} \right)_P A_{f-fP}^x + \left( v_P^* - d_u \frac{\partial p'}{\partial y} \right)_P A_{f-fP}^y \right] \end{aligned} \quad (11b)$$

Additionally, since the velocity  $u$  and  $v$  in the semi-staggered grid are arranged at the same position at the cartesian coordinate, the coefficients of the discrete equation of  $u$  and  $v$  are the same with each other, except for the constant term. Thus, with this equality, the coupling coefficients of pressure and velocity,  $d_u$  and  $d_v$ , can be both presented as  $d_u$  in Eq. (11b). It should be noted that the coupling coefficient of pressure and velocity in Eq. (10) or Eq. (11) is different from that in Ref. [1]. The former can be regarded as the diffusion or heat conduction coefficient of the diffusive equation, while the latter is equivalent to the heat transfer coefficient. Therefore, the pressure-correction contribution towards the flow flux through the interface can be discrete in the same way as the diffusion terms.

It's difficult to establish the discrete pressure-correction equation, where the pressure gradient in the velocity control volume is related to all pressure values of the vertex contained in the basic cell. Similar to the treatment in the traditional staggered grid, the assumption that the computation of pressure gradient at the interface of the control volume only involves the pressure values besides the interface. Meantime, it is assumed that when calculating the flux flowing through the boundary the pressure control volume  $FP$ , the gradient of the pressure-correction values at  $P$  and  $F$  are identical and both equal to the pressure gradient at the interface  $FP$ , as shown in Eq. (12).

$$\begin{cases} \left( \frac{\partial p'}{\partial x} \right)_F = \left( \frac{\partial p'}{\partial x} \right)_P = \left( \frac{\partial p'}{\partial x} \right)_f \\ \left( \frac{\partial p'}{\partial y} \right)_F = \left( \frac{\partial p'}{\partial y} \right)_P = \left( \frac{\partial p'}{\partial y} \right)_f \end{cases} \quad (12)$$

Then the mass flux formula through  $PF$  can be transformed into

$$m_f = [\beta_f \rho_F u_F^* + (1 - \beta_f) \rho_P u_P^*] A_{FP}^x + [\beta_f \rho_F v_F^* + (1 - \beta_f) \rho_P v_P^*] A_{FP}^y - [\beta_f \rho_F (d_u)_F + (1 - \beta_f) \rho_P (d_u)_P] \left( (\nabla p')_f \cdot \vec{A}_{FP} \right) \quad (13)$$

where  $\beta = \frac{|\vec{fP}|}{|\vec{FP}|}$ ,  $\vec{A}_{FP} = (y_P - y_F, x_F - x_P)$ ,  $\vec{A}_{Ff} = (A_{Ff}^x, A_{Ff}^y) = (y_f - y_F, x_F - x_f)$ . It can be found that the last term of the flow flux formula holds the same form as the diffusion term, thus the same discrete format can be adopted to treat this term, as shown in Eq. (14).

$$\left( (\nabla p')_f \cdot \vec{A}_{FP} \right) = D_j (p'_j - p'_i) + \overline{\nabla p'} \cdot \vec{A}_f^{cross} \quad (14)$$

where  $\vec{A}_f^{cross} = \vec{A}_{FP} - D_j \vec{ij}$ ,  $i \vec{j} = (x_j - x_i, y_j - y_i)$ .

The discrete pressure-correction equation can be obtained:

$$a_i p'_i = \sum_j^{Ng} a_j p'_j + b_i \quad (15)$$

where  $a_i = \sum_j^{Ng} a_j$ ,  $a_j = [\beta_f \rho_F (d_u)_F + (1 - \beta_f) \rho_P (d_u)_P] D_j$ , and

$$b_i = - \sum_f^{N_f} m_f^* + \sum_f^{N_f} \left\{ [\beta_f \rho_F (d_u)_F + (1 - \beta_f) \rho_P (d_u)_P] \left( (\nabla p')_f \cdot \vec{A}_{FP}^{cross} \right) \right\}_f - \sum_{fb}^{N_{fb}} m_{fb}^*$$

The subscript  $fb$  stands for the vertex at the boundary, and  $m_{fb}^*$  is the mass flux flowing into the control volume  $i$ , and  $N_{fb}$  is the number of boundary interfaces of the pressure-correction control volume. Obviously, the mass flux  $m_{fb}^*$  equals to zero for the interior control volume. The boundary control volume  $i$  is shown in Fig. 2, which contains two boundary interfaces:  $if^i$  and  $f_1 i$ .

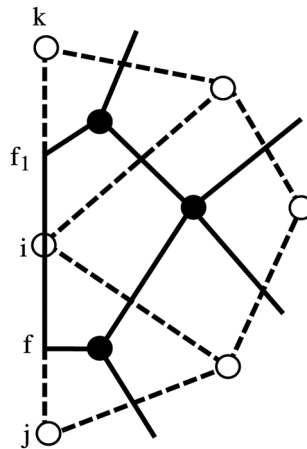


**Figure 2:** Boundary control volume for the pressure-correction equation

The effect of the pressure-correction gradient in the mass conservation equation can only be dealt with explicitly and solved through iteration. Generally, the effect can be ignored in the calculation unless the grid is very oblique. The computation cost by employing the model proposed in this paper is not very large because the velocity is arranged in the center of the basic cell. After getting the pressure-correction information, the

pressure gradient of the basic cell can be figured out to update the velocity. To achieve the purpose of solving the mass conservation equation, sometimes the pressure correction equation needs to be solved twice, which in return would lead to the increased computational resource for calculating the right end vector and the pressure correction equation. In the case of relatively oblique mesh, it is necessary to consider this dealing method.

## 6 Calculation of Pressure Gradient and Correction of Velocity for Basic Cell

After getting the pressure-correction values of vertexes, the Gauss-Green theorem is employed to calculate the pressure gradient or the pressure-correction gradient for basic cell

$$\left(\frac{\partial p'}{\partial x}\right)_P = \frac{1}{2\Delta_v} \sum_g^{N_g} (p'_i + p'_j)_g A_g^x$$

$$\left(\frac{\partial p'}{\partial y}\right)_P = \frac{1}{2\Delta_v} \sum_g^{N_g} (p'_i + p'_j)_g A_g^y$$
(16)

where  $i$  and  $j$  represent two vertexes at the interface of the cell  $g$ . The update of velocity can be shown as

$$u_P = u_P^* - (d_u)_P \left(\frac{\partial p'}{\partial x}\right)_P$$

$$v_P = v_P^* - (d_v)_P \left(\frac{\partial p'}{\partial y}\right)_P$$
(17)

It can be seen that the coupling between pressure and velocity in the semi-staggered grid behaves in a relatively natural and close manner. The approximation of the pressure gradient on the interface of the pressure control volume is identical to the classical structured-grid. Meantime, the identical velocity field is used to satisfy the conservation equation of mass and of momentum.

The semi-staggered arrangement on the unstructured grid requires larger memory than the collocated grid to save the geometric information of the basic cell and the corresponding dual polygons. However, the code related to that geometric information only needs to run once, which would impose no influence on the speed of calculation. The steps of this algorithm are the same as the SIMPLE algorithm and further details are not included here.

## 7 Results and Discussion

In this section, several numerical cases are presented to verify the effectiveness of the algorithm, including the lid-driven flow, the natural convection in a square cavity, the flow in a channel with 180° bend and Kovaszay precise solution.

### 7.1 Lid-Driven Flow

The lid-driven flow is a relatively classical numerical test case. The geometric model of lid-driven flow is depicted in Fig. 3, and the corresponding grid used for calculation is shown in Fig. 4. Ghia et al. [12] calculated this problem under the condition of Reynold number ranging from 400 to 10000 and the zero angle of inclination, using the vortex-flow function method and multigrid technique on a mesh system from  $129 \times 129$  to  $257 \times 257$ , where the results of velocity at the horizontal and the vertical centerline and different diagrams of the vortex-flow function were presented in this work. By comparing the numerical results of velocity at two central lines with the date from Ghia's [12] work, the present numerical method is validated.

Figs. 5–7 presents good agreement between the numerical results from the semi-staggered grid and the data from Chia et al. [12] even in high Reynolds number conditions. There are two reasons for the slight

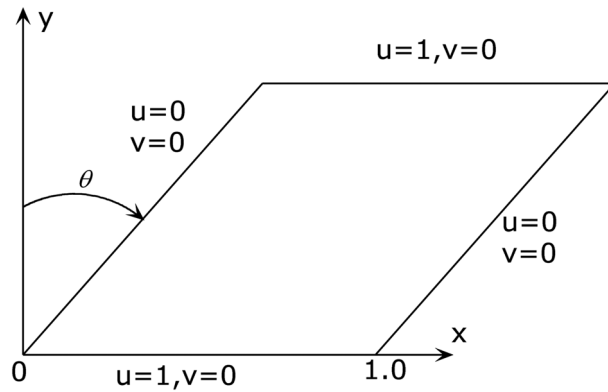


Figure 3: Geometric model of lid-driven flow

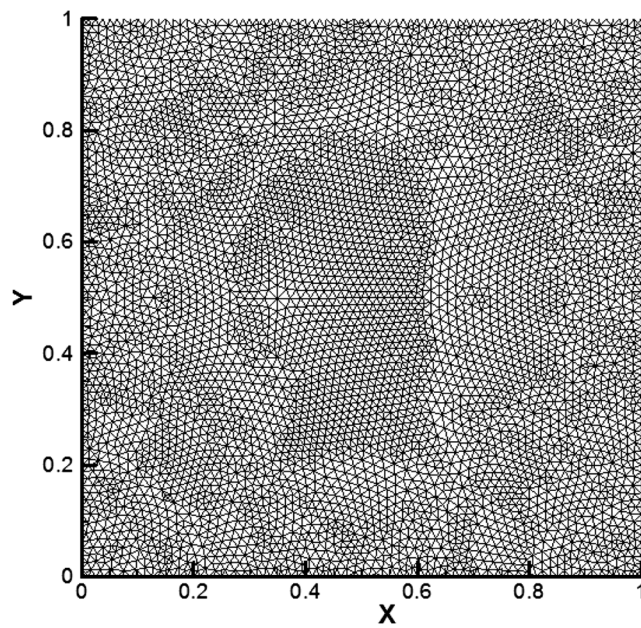


Figure 4: Grid for lid-driven flow (9978 cells and 5150 vertexes)

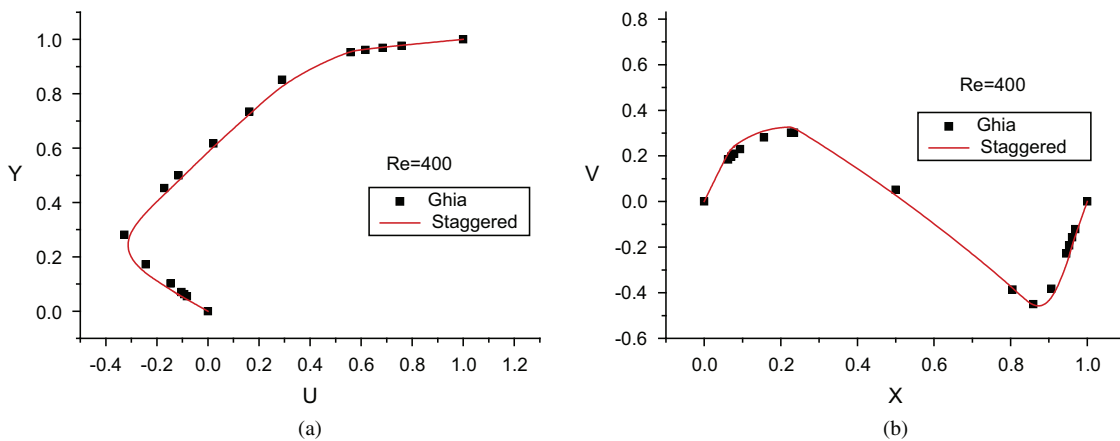
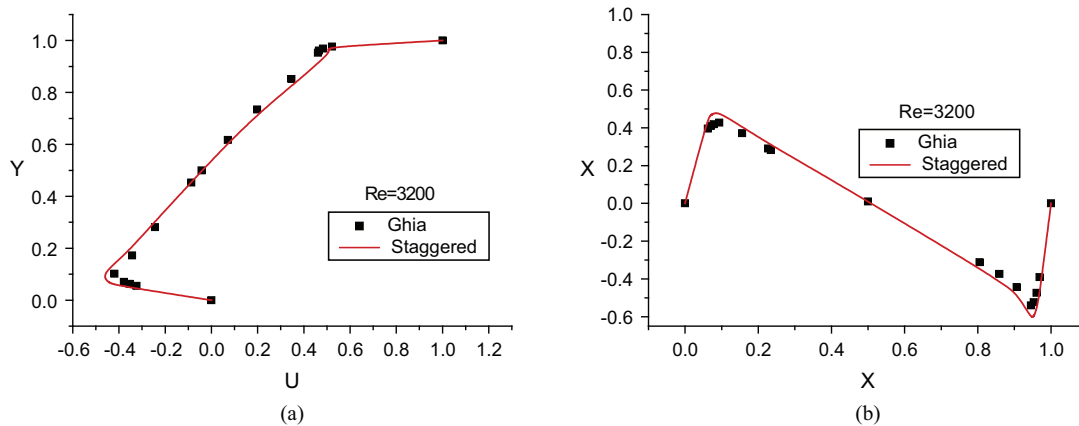
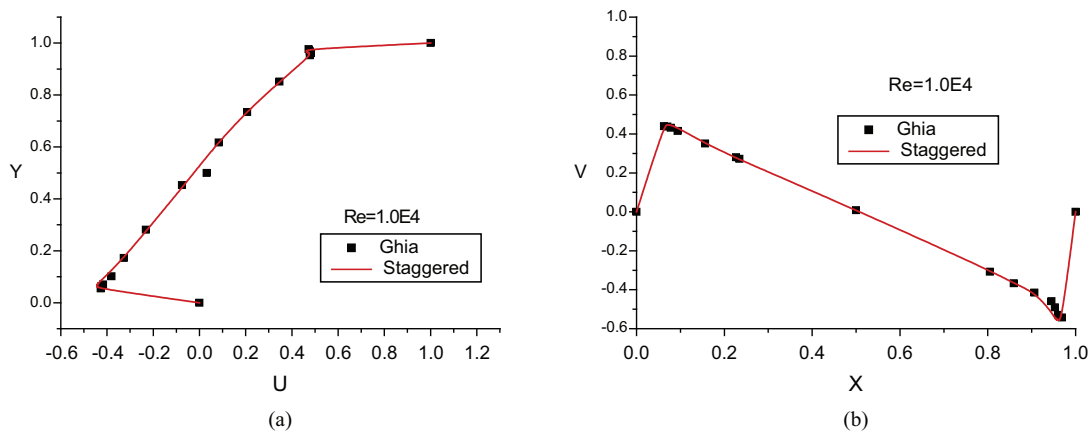


Figure 5: Comparison of velocity at the central line,  $Re = 400$ . (a) Velocity component at the vertical central line. (b) Velocity component at the horizontal central line



**Figure 6:** Comparison of velocity at the central line,  $Re = 3200$ . (a) Velocity component at the vertical central line. (b) Velocity component at the horizontal central line



**Figure 7:** Comparison of velocity at the central line,  $Re = 10000$ . (a) Velocity component at the vertical central line. (b) Velocity component at horizontal central line

difference between the numerical results from the semi-staggered grid and the benchmark solution. Firstly, compared with 16384 rectangular cells used in Chia's work, only 9978 triangular cells are employed in this numerical case. The fewer cells leads to the inferior degree of orthogonality and the less uniformity of cells, which in return will have an adverse effect on the precision of numerical results. The other reason is that the velocity distribution on the center face is obtained by the interpolation method, which will introduce some errors.

In order to test the adaptability of this semi-staggered oblique grid, different values of  $\theta$  in Fig. 3 are selected to execute the computation. The examination shows that the algorithm can work well even in  $\theta = 80^\circ$ . The velocity vector distribution presented in Fig. 8 with  $\theta = 75^\circ$  and  $Re = 104$  proves that the semi-staggered technique can be applied in the extraordinary oblique grid. As there is no report about the velocity distribution at the central line under the oblique situation, the comparison is not included here.

## 7.2 Natural Convection in a Square Cavity

Natural convection in a square cavity is an issue of flow and heat transfer in an enclosed domain, where the flow driving force is buoyancy force from the fluid density difference caused by the temperature gradient.

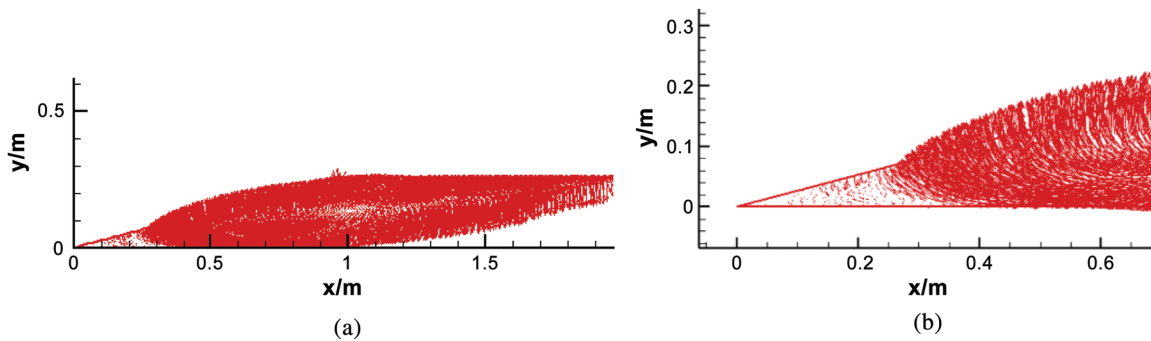


**Figure 8:** Velocity vector distribution with high Re and oblique situation. (a) Global velocity vector distribution. (b) Local velocity vector distribution at the left bottom

It is assumed that the fluid is subject to the Boussinesq hypothesis. The computational domain is set as a square area with the height and width equal to 1, while the adiabatic boundary condition (the second homogeneous boundary condition) is imposed on the top and the bottom boundary. The isothermal boundary condition (the first boundary condition) is applied on the left and the right boundaries with different temperatures. The comparison between the numerical results calculated with the grid shown in Fig. 4 and the results from reference [13] is presented in Tab. 1.

**Table 1:** Numerical results of natural convection in a square cavity with grid NE = 9978, NP = 5470,  $\alpha_u = \alpha_v = 0.85$ , and  $\alpha_p = 0.275$

Ra	$10^3$	$10^4$	$10^5$	$10^6$	$10^7$
iteration	1685	863	619	485	926
CPU/s	197.34	110.06	82.06	66.36	117.68
Nu	1.1186	2.2483	4.5260	8.8150	15.716
Nu [7]	1.114	2.245	4.510	8.806	—————

Where Rayleigh number  $Ra = \alpha g(T_h - T_c)H^3 / (\nu\alpha)$ .  $\alpha$  represents the coefficient of thermal expansion of fluid.  $g$  is gravitational acceleration.  $T_h$  and  $T_c$  are the temperatures of the left and the right side of the square cavity.  $H$  is the height of the square cavity.  $\alpha$  stands for the thermal diffusion coefficient, and  $\nu$  is the kinematic viscosity. Results in Tab. 1 show that the maximum difference between the numerical computation and data from the reference is less than 0.5%.

### 7.3 Flow in a Channel with 180° Bend

Date et al. [14] presented the geometric description of this test case and the pressure distributions of the inner and outer of the flow channel. In their research, the complete pressure correction algorithm for the solution of incompressible flow based on the collocated grid is employed. The geometric model and the flow conditions in a channel with 180° bent are shown in Figs. 9 and 10, which is a numerical example of a highly nonlinear internal pressure distribution. Since only the pressure distribution curve is presented in Date's work, while no specific data of pressure distribution is reported, so the comparison of the inner and outer pressures just involves the pressure distribution curve. There are some peaks on the pressure profiles along the inner wall and outer wall, these peaks correspond to the bent corners where the flow direction is changed 90 degree.

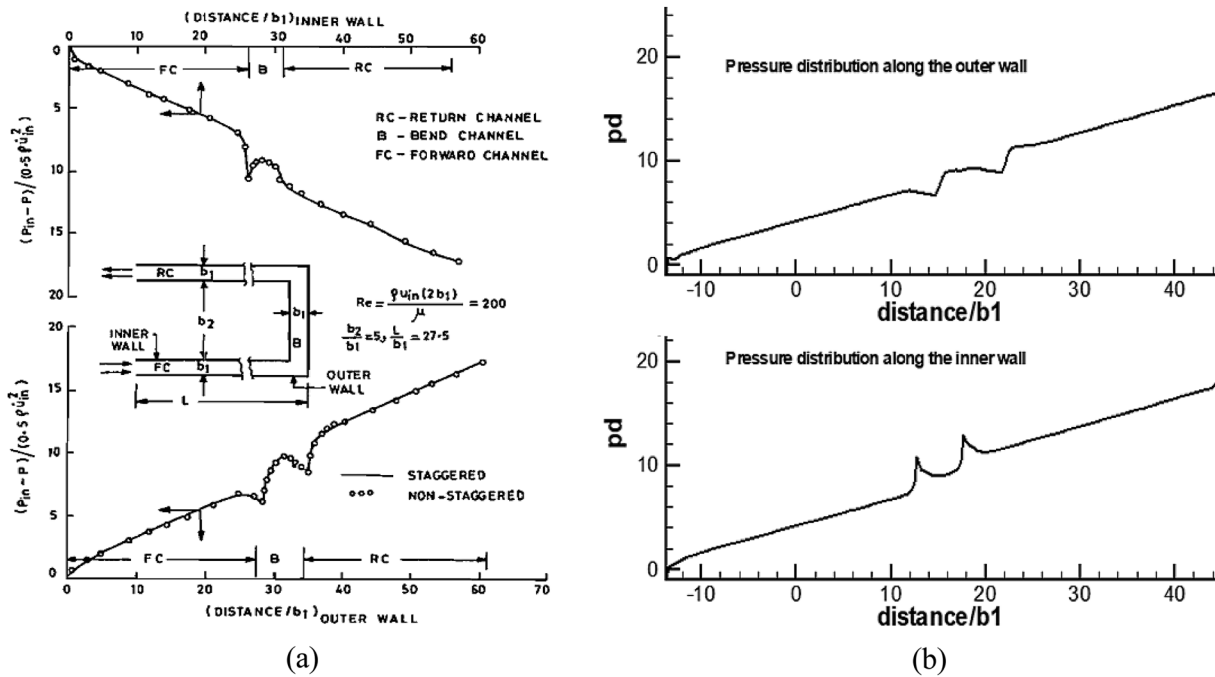


**Figure 9:** Geometric model of flow in a channel with 180° bend and comparison of the inner and outer pressure distribution curve. (a) Pressure distribution curve in Date et al. [14]. (b) Pressure distribution curve

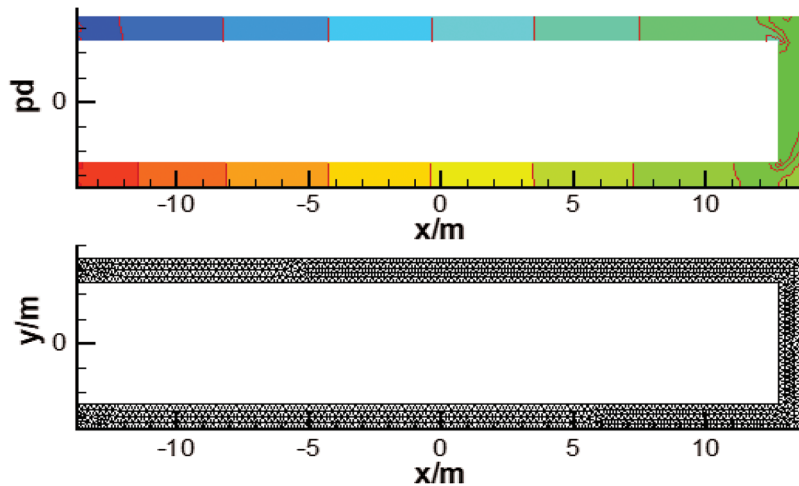


**Figure 10:** Pressure contour distribution and the corresponding grid

It is challenging for the algorithm to calculate the flow in a channel with 180° bend because of the existence of the strong nonlinear pressure distribution and 180° reverse of velocity in the channel. The pressure distribution and the pressure fluctuation caused by the shape change of the flow channel are presented. The numerical results of this paper present a good agreement with the results of Date's [14].

#### 7.4 Kovaszny Accurate Solution

Kovaszny flow is a steady incompressible Navier-Stokes (NS) flow problem with an analytic solution [15]. Rebholz et al. [16] demonstrated that it is indeed the solution of the steady and constant property NS

equation without source term, and the expression is shown in Eq. (18). In the process of numerical calculation, the quadrilateral structured grid is employed for calculation, and the boundary conditions are determined by the analytical solution while the physical properties remain constant.

$$\begin{cases} u = 1 - e^{\lambda x} \cos(2\pi y) \\ v = \frac{\lambda e^{\lambda x}}{2\pi} \sin(2\pi y) \\ p = p_0 - \frac{e^{2\lambda x}}{2}, \lambda = \frac{Re}{2} - \sqrt{\frac{Re^2}{4} + 4\pi^2} \end{cases} \quad (18)$$

where the kinematic viscosity  $\nu = \mu/\rho = 1/Re$ . Since the analytic solution is available in this case, the  $L_2$  norm, as shown in Eq. (19), is chose to check the accuracy of numerical results.

$$L_2-\phi = \sqrt{\sum_{i=1}^N (\phi_i^n - \phi_i^a)^2} / N \quad (19)$$

In Eq. (19),  $\phi_i^n$  and  $\phi_i^a$  stand for the numerical solution and the exact solution at the position  $i$ , respectively.  $\phi$  represents the velocity component  $u$  or  $v$ , and  $N$  is the number of grid cells. The  $L_2$  norm is the average distance of the exact solution vector and the numerical solution vector. It also means the average error of the numerical solution. The flow function is presented in Fig. 11.

The variations of  $L_2$  norm with the calculating grid cells are shown in Tab. 2. Tab. 2 shows that the numerical results obtained from the semi-staggered grid technique are in good agreement with the accurate solution, with the maximum relative error smaller than  $3.07 \times 10^{-4}$ .

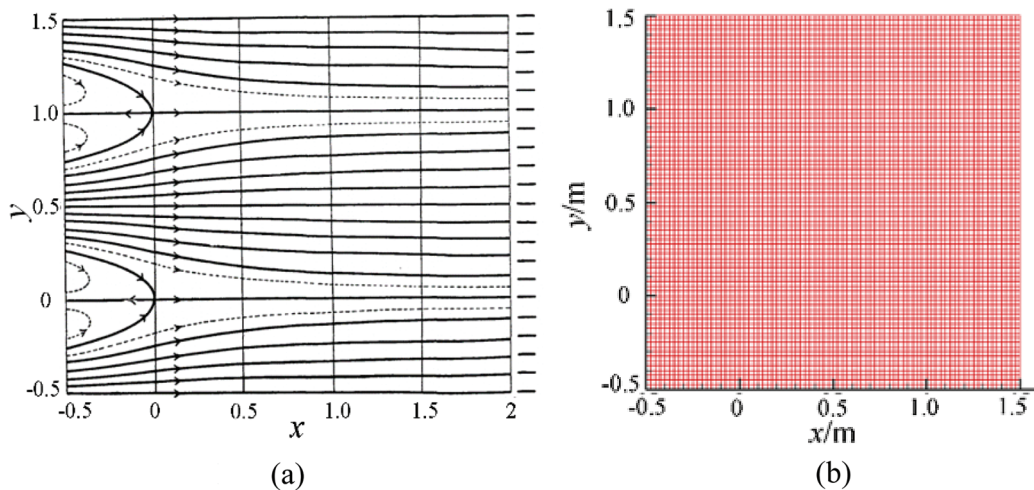


**Figure 11:** Flow function and the corresponding grid. (a) Flow function. (b) Grid

**Table 2:** Variation of  $L_2$  norm with the grid cells

Number of grid cells	$L_2$ norm of $u$	$L_2$ norm of $v$
1600	$3.07 \times 10^{-4}$	$6.74 \times 10^{-5}$
6400	$3.99 \times 10^{-5}$	$7.75 \times 10^{-6}$
25600	$5.05 \times 10^{-6}$	$9.60 \times 10^{-7}$

## 8 Conclusions

The semi-staggered grid arrangement with the pressure at the vertex and the other variables at the center of the cell is proved feasible in this paper. The semi-staggered grid technique is employed to solve several classical testing cases. Results show that the semi-staggered grid technique can be applied to solve the flow and heat transfer problem with high Reynolds number and the inclined grid. This semi-staggered arrangement technique is suitable for generating the quadrilateral grid, and even the triangular grid. For the triangular grid, it has the advantage of reducing the computational resource for solving the pressure-correction equations, since the number of triangular grid vertex is about half of the number of cells.

**Funding Statement:** This work was financially supported by the Natural Science Foundation of China (No. 51676208) and the Fundamental Research Funds for the Central Universities (No. 18CX07012A and No. 19CX05002A). The authors are also grateful for the support from the Major Program of the Natural Science Foundation of Shandong Province (No. ZR2019ZD11).

**Conflicts of Interest:** The authors declare that they have no conflicts of interest to report regarding the present study.

## References

1. Patankar, S. V. (1980). *Numerical heat transfer and fluid flow*. Hemisphere Publishing Corporation, USA.
2. Rhie, C. M., Chow, W. L. (1983). Numerical study of the turbulent flow past an airfoil with trailing edge separation. *AIAA Journal*, 21(11), 1525–1532. DOI 10.2514/3.8284.
3. Williams, M. (1993). The solution of the two-dimensional incompressible flow equations on unstructured triangular meshes. *Numerical Heat Transfer*, 23(3), 309–325. DOI 10.1080/10407799308914903.
4. Davidson, L. (1996). A pressure correction method for unstructured meshes with arbitrary control volumes. *International Journal for Numerical Methods in Fluids*, 22(4), 265–281. DOI 10.1002/(SICI)1097-0363(19960229)22:4<265::AID-FLD359>3.0.CO;2-J.
5. Mathur, S. R., Murthy, J. Y. (1997). A pressure-based method for unstructured meshes. *Numerical Heat Transfer*, 31(2), 195–215. DOI 10.1080/10407799708915105.
6. Lai, Y. G. (1997). An unstructured grid method for a pressure-based flow and heat transfer solver. *Numerical Heat Transfer*, 32(3), 267–281. DOI 10.1080/10407799708915009.
7. Kawaguchi, Y., Tao, W. Q., Ozoe, H. (2002). Checkerboard pressure predictions due to the underrelaxation factor and time step size for a nonstaggered grid with momentum interpolation method. *Numerical Heat Transfer: Part B: Fundamentals*, 41(1), 85–94. DOI 10.1080/104077902753385027.
8. Katz, A., Sankaran, V. (2011). Mesh quality effects on the accuracy of CFD solutions on unstructured meshes. *Journal of Computational Physics*, 230(20), 7670–7686. DOI 10.1016/j.jcp.2011.06.023.
9. Xue, S. C., Barton, G. W. (2013). A finite volume formulation for transient convection and diffusion equations with unstructured distorted grids and its applications in fluid flow simulations with a collocated variable arrangement. *Computer Methods in Applied Mechanics and Engineering*, 253, 146–159. DOI 10.1016/j.cma.2012.09.016.
10. Thomadakis, M., Leschziner, M. (1996). A pressure-correction method for the solution of incompressible viscous flows on unstructured grids. *International Journal for Numerical Methods in Fluids*, 22(7), 581–601. DOI 10.1002/(SICI)1097-0363(19960415)22:7<581::AID-FLD365>3.0.CO;2-R.
11. Hwang, Y. H. (1995). Calculations of incompressible flow on a staggered triangular grid, part II: applications. *Numerical Heat Transfer*, 27(3), 337–353. DOI 10.1080/10407799508914961.
12. Peters, S., Maliska, C. R. (2017). A staggered grid arrangement for solving incompressible flows with hybrid unstructured meshes. *Numerical Heat Transfer, Part B: Fundamentals*, 71(1), 50–65. DOI 10.1080/10407790.2016.1257221.
13. Jasak, H. (1996). *Error analysis and estimation for the finite volume method with applications to fluid flows (Ph.D. Thesis)*. Imperial College of Science, UK.

14. Ghia, U., Ghia, K. N., Shin, C. T. (1982). High-Re solutions for incompressible flow using the Navier-Stokes equations and a multigrid method. *Journal of Computational Physics*, 48(3), 387–411. DOI 10.1016/0021-9991(82)90058-4.
15. Tao, W. Q. (2001). *Numerical heat transfer. 2 nd ed.* Xi'an Jiaotong University Press, China.
16. Date, A. W. (1996). Complete pressure correction algorithm for solution of incompressible Navier-Stokes equations on a nonstaggered grid. *Numerical Heat Transfer*, 29(4), 441–458. DOI 10.1080/10407799608914991.
17. Kovasznay, L. I. G. (1948). Laminar flow behind a two-dimensional grid. *Mathematical Proceedings of the Cambridge Philosophical Society*, 44(1), 58–62. DOI 10.1017/S0305004100023999.
18. Rebholz, L. G., Watro, S. A. (2014). A note on Taylor-Eddy and Kovasznay solutions of NS- $\alpha$ -deconvolution and Leray- $\alpha$ -deconvolution models. *Journal of Nonlinear Dynamics*, 2014(1), 1–5. DOI 10.1155/2014/959038.
19. Jalali, A., Sharbatdar, M., Ollivier-Gooch, C. (2016). An efficient implicit unstructured finite volume solver for generalised Newtonian fluids. *International Journal of Computational Fluid Dynamics*, 30(3), 201–217. DOI 10.1080/10618562.2016.1188202.
20. Darwish, M., Mangani, L., Moukalled, F. (2017). General fully implicit discretization of the diffusion term for the finite volume method. *Numerical Heat Transfer, Part B: Fundamentals*, 71(6), 506–532. DOI 10.1080/10407790.2017.1330060.
21. Sezai, I. (2017). Implementation of boundary conditions in pressure-based finite volume methods on unstructured grids. *Numerical Heat Transfer, Part B: Fundamentals*, 72(1), 82–107. DOI 10.1080/10407790.2017.1338077.